Original Article
ISSN (Online): 2582-7472

ShodhKosh: Journal of Visual and Performing Arts
January 2024 5(1), 1487–1514

EFFECT OF SURFACE ROUGNESS ON FINITE POROUS JOURNAL BEARING LUBRICATION OF MICROPOLAR FLUID WITH SQUEEZING EFFECT

Santosh Huggi [1]

[1] Department of Mathematics, Associate Professor, Government First Grade College, Afzalpur, Karnataka., India

ABSTRACT

In this paper, a theoretical analysis of the effect of surface roughness on the squeeze film lubrication of finite porous journal bearings with micropolar fluids is studied. A more generalized form of surface roughness is mathematically modeled by a stochastic random variable with non-zero mean, variance and skewness. The generalized average Reynolds type equation is derived for the squeeze film lubrication of finite rough porous journal bearings with micropolar fluids as lubricant. The closed form expressions are obtained for the fluid film pressure, load carrying capacity, journal centre velocity and locus of the journal centre. The cases of a constant applied load and an alternating applied load are analyzed under a cyclic load the micropolar fluids provide a reduction in the journal centre velocity. Further, it is numerical computations of the results show that the negatively skewed surface roughness pattern increase fluid film pressure, load carrying capacity and decreases the journal centre velocity. Where as adverse effects were found for the positively skewed surface roughness pattern. The effect of porous parameter causes reduction in fliud film pressure, load carrying capacity and enhances the journal centre velocity.

Keywords: Nomenclature

c	radial clearance
c^*	maximum deviation from the mean film thickness
e	eccentricity
E	expectancy operator
h(θ)	mean film thickness (h=c+e cos⁡θ)
h_s	random variable
h¯	non-dimensional film thickness (= h/c)
h¯_0	minimum film height
H	film thickness (=h(θ)+h_s)
H_0	porous layer thickness
k	permeability of the porous matrix
l	characteristic length of the polar suspension (=(γ/4μ)^(1/2))
l¯	non-dimensional form of l (= l/c)

Corresponding Author

Santosh Huggi, huggiss1979@gmail.com

DOI
10.29121/shodhkosh.v5.i1.2024.3488

Funding: This research received no specific grant from any funding agency in the public, commercial, or not-for-profit sectors.

L	bearing length
N	coupling number (=(χ/(χ+2μ))^(1/2))
p	lubricant pressure
$\bar{p}$	non-dimensional pressure (=(E(p) c^2)/(μR^2 (∂ε/∂t)))
R	radius of the journal
t	time
u,v,w	components of fluid velocity in x, y and z directions, respectively
v_1,v_2,v_3	microrotational velocity components in the x , y and z directions
r,θ,z	cylindrical co-ordinates
V	squeeze velocity, ∂H/∂t (=c ∂ε/∂t cosθ)
W(s)	steady load
W(t)	applied load
$\bar{W}$	non-dimensional load carrying capacity (=(E(W_s) c^2)/(μLR^3 (∂ε/∂t)))
W_0	amplitude of the applied cyclic load
$\bar{W}$(s)	mean steady load
S	sommerfeld number (=((μN))/((E(W_0)/2LR))×(R/c)^2)
x,y,z	Cartesian co-ordinates
α	non-dimensional form of α (=α^*/c)
α^*	mean stochastic film thickness
σ^2	non-dimensional form of (=σ^(*^2)/c^2)
〖σ^*〗^2	variance
ε	eccentricity ratio (= e/c)
ε_1	non-dimensional form of ε_1 (=ε^*/c^3)
ε^*	measure of symmetry of the stochastic random variable.
χ	spin viscosity
γ	viscosity co-efficient for micropolar fluids
μ	viscosity co-efficient
τ	dimensionless response time (=(2πN/60 t))

ψ	permeability parameter (= kH0/c3)
θ	circumferential co-ordinate (= x/R)
λ	length to diameter ratio (=L/2R)
ω	frequency of applied cyclic load
Δ	gradient operator

1. INTRODUCTION

The journal bearings have been extensively studied for a long time. In most of the studies the common assumptions made where, the lubricants are Newtonian and the bearing surfaces are perfectly smooth. However, these assumptions are unrealistic as most of the modern lubricants are non-Newtonian in their character and all bearing surfaces are rough on mircoscale. Even early attempts to develop a theory of friction recongnized the fact that all practically prepared surfaces are rough on the microscopic scale. The aspect ratio and the absolute height of the asperities and vallys observed under the microscope very greatly, depending on material properties and on the method of surface preparation surface roughness height may range from 0.05 μ m or less on polished surface to 10 μ m on medium machined surfaces. For the past few decades the trend has been towards the increasing of viscosity index to manifolds. This is due to the fact that, base oils with high viscosity index exhibit improved response to additives of various chemical compositions which upgrades their quality and makes for reduced additives consumption in the production of additives blended oils. Thus, the current paper presents theoretical study of non-Newtonian behaviour of the lubricants by considering Eringen [1] constitive equations for the micropolar fluids. Micropolar fluids contain a suspension of particles with individual motion. These particles support stress and body moments [1-2] and are subject to spin inertia and hence microscopic effects generated by the local structure and micro motion of fluid elements are exhibited. This fliud model is applicable for the study of flow properties of non-Newtonian fluids such as polymers, paints, lubricants, suspended fluids, blood etc. The micropolar fluids theory has been used by several investigators for the study of different bearing systems such as journal bearings [3-5], Slider bearings [6-7], Squeeze film bearings [8-12] and porus bearings [13-15]. These studies revealed some of the advantages of micropolar fluids over the Newtonian lubricants, such as increased load carrying capacity and delayed time of approach for squeeze film bearings. The effect of surface roughness on the hydrodynamic lubrication of bearings has been studied by several investigators. The random character of the surface roughness prompted several researchers to adopt a stochastic approach to model a surface roughness [16-17]. The stochastic model developed by a christensen [15] for the study of hydrodynamic lubrication of rough surfaces formed the basis for several studies [18-21]. In recently Naduvinamani et.al [22-23] studied the hydrodynamic lubrication of journal bearings by including the micropolar lubricants. Hence in the present paper, the surface roughness on the bearing surface is modeled by a stochastic random variable with non-zero mean, variance and skewness.

2. MATHEMATICAL FORMULATION OF THE PROBLEM

The physical configuration of the problem under consideration is shown in the figure 1. The journal of radius R approaches the porous bearing surface at a circumferential section, θ with a given velocity, $V\left(=\frac{\partial H}{\partial t}\right)$. The lubricant in the film region is assumed to be micropolar fluid [1]. For the mathematical representation of the surface roughness, the fluid film thickness H is considered to be consisting of two parts and is given by

$$H = h(\theta) + h_s \qquad (1)$$

where $h(\theta) = c(1+\varepsilon\cos\theta)$ is the mean film thickness. '*c*' is radial clearance and 'ε' is the eccentricity ratio parameter, and h_s is a randomly varying quantity measured from the

mean level and this characterizes the surface roughness of the bearing.

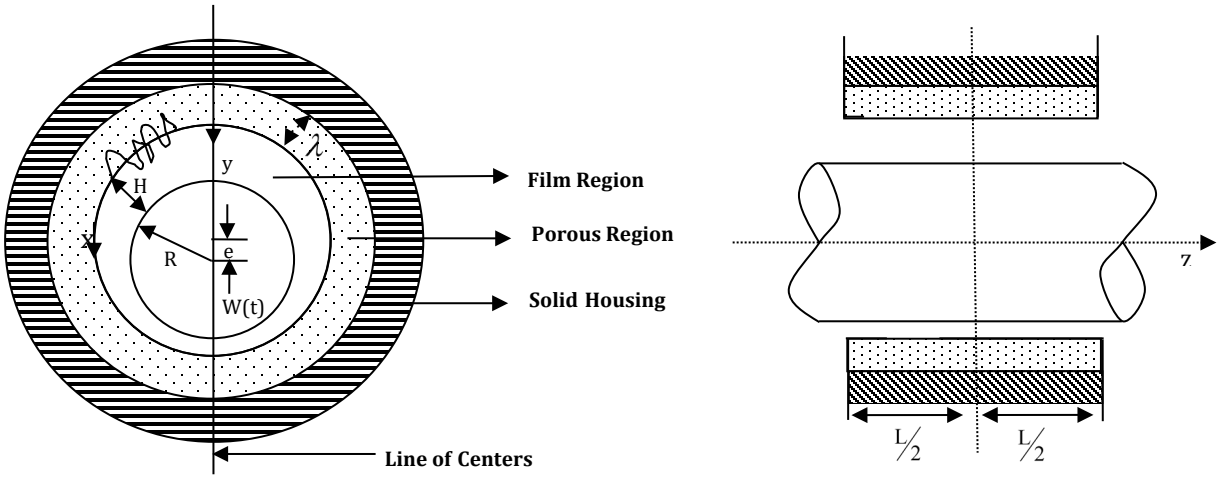

Figure 1. Physical configuration of a finite porous journal bearing.

Let $f(h_s)$ be the probability density function defined over the domain $-c^* \le h_s \le c^*$ where c^* being maximum deviation from the mean film thickness. The mean α^*, standard deviation σ^* and the parameter ε^*, which is measure of the symmetry of random variable h_s are defined as [24].

$$\alpha^* = E(h_s) \tag{2}$$

$$\sigma^{*2} = E\left[\left(h_s - \alpha^*\right)^2\right] \tag{3}$$

$$\varepsilon^* = E\left[\left(h_s - \alpha^*\right)^3\right] \tag{4}$$

Where *E* is an expectancy operator defined by

$$E(\bullet) = \int_{-\infty}^{\infty} (\bullet) f(h_s)\, dh_s \tag{5}$$

It is to be noted that, the parameters α^*, σ^* and ε^* are independent of *x*. The mean α^* and parameter ε^* can assume both positive and Negative values, however, σ^* can always assume positive values. The particular case of $\varepsilon^* = 0$ refers to the symmetrical distribution, negatively values of ε^* refers to negatively skewed surface roughness and positive values of ε^* refers to positively skewed surface roughness pattern on the bearing surface.

The constitutive equations for micropolar fluids proposed by Eringen [2] simplify considerably under the usual assumptions of hydrodynamic lubrication. The resulting equations under steady–state conditions are

Conservation of linear momentum:

$$\left(\mu + \frac{\chi}{2}\right)\frac{\partial^2 u}{\partial y^2} + \chi\frac{\partial v_3}{\partial y} - \frac{\partial p}{\partial x} = 0\,, \tag{6}$$

$$\left(\mu + \frac{\chi}{2}\right)\frac{\partial^2 w}{\partial y^2} - \chi\frac{\partial v_1}{\partial y} - \frac{\partial p}{\partial y} = 0\,. \tag{7}$$

Conservation of angular momentum:

$$\gamma \frac{\partial^2 v_1}{\partial y^2} - 2\chi v_1 + \chi \frac{\partial w}{\partial y} = 0 \ , \qquad (8)$$

$$\gamma \frac{\partial^2 v_3}{\partial y^2} - 2\chi v_3 - \chi \frac{\partial u}{\partial y} = 0 \ . \qquad (9)$$

Conservation of mass:

$$\frac{\partial u}{\partial x} + \frac{\partial v}{\partial y} + \frac{\partial w}{\partial z} = 0 \qquad (10)$$

Where (u, v, w) are the velocity components of the lubricant in the *x*, *y* and *z* directions, respectively, and (v_1, v_2, v_3) are micro rotational velocity components, χ is the spin viscosity and γ is the viscosity coefficient for micropolar fluids and μ is the Newtonian viscosity coefficient.

The flow of micropolar lubricants in a porous matrix governed by the modified Darcy law, which account for the polar effects is given by [25]

$$\vec{q}^{\,*} = \frac{-k}{(\mu + \chi)} \nabla p^* \qquad (11)$$

Where $\vec{q}^{\,*} = \left(u^*, v^*, w^*\right)$ is the modified Darcy velocity vector, with

$$u^* = \frac{-k}{(\mu+\chi)} \frac{\partial p^*}{\partial x} \quad , \quad v^* = \frac{-k}{(\mu+\chi)} \frac{\partial p^*}{\partial y} \quad , \quad w^* = \frac{-k}{(\mu+\chi)} \frac{\partial p^*}{\partial z} \qquad (12)$$

k is the permeability of the porous matrix and p^* is the pressure in the porous region.

Due to continuity of fluid in the porous matrix, p^* satisfies the Laplace Equation.

$$\frac{\partial^2 p^*}{\partial x^2} + \frac{\partial^2 p^*}{\partial y^2} + \frac{\partial^2 p^*}{\partial z^2} = 0 \qquad (13)$$

The relevant boundary conditions are

at the bearing surface $(y = 0)$

$$u = 0, \ v = v^* \ , \ w = 0 \qquad (14a)$$

$$v_1 = 0 \ , \ v_3 = 0 \qquad (14b)$$

at the journal surface $(y = H)$

$$u = 0, \ v = \frac{\partial H}{\partial t} \ , \ w = 0 \qquad (15a)$$

$$v_1 = 0 \ , \ v_3 = 0 \qquad (15b)$$

3. SOLUTION OF THE PROBLEM

The generalized Reynolds equation is given by [23]

$$\frac{\partial}{\partial x}\left[\left(f(N,l,H) + \frac{12\,\mu k H_0}{(\mu+\chi)}\right)\frac{\partial p}{\partial x}\right] + \frac{\partial}{\partial z}\left[\left(f(N,l,H) + \frac{12\,\mu k H_0}{(\mu+\chi)}\right)\frac{\partial p}{\partial z}\right] = 12\,\mu \frac{\partial H}{\partial t} \qquad (16)$$

Where $f(N,l,H)=H^3+12l^2H-6NlH^2\coth\left(\frac{NH}{2l}\right)$, $\frac{\partial H}{\partial t}=c\frac{\partial\varepsilon}{\partial t}\cos\theta$.

Multiplying both sides of equation (16) by $f(h_s)$ and integrating with respect to h_s from $-c^*$ to c^* and also using equations (2) to (4), the averaged modified Reynolds equation is obtained in the form

$$\frac{\partial}{\partial x}\left[E\left(f(N,l,H)+\frac{12\mu k H_0}{(\mu+\chi)}\right)\frac{\partial E(p)}{\partial x}\right]+\frac{\partial}{\partial z}\left[E\left(f(N,l,H)+\frac{12\mu k H_0}{(\mu+\chi)}\right)\frac{\partial E(p)}{\partial z}\right]=12\mu\frac{\partial E(H)}{\partial t} \quad (17)$$

Where

$F(N,l,h)=E[f(N,l,H)\approx F_1+F_2(F_3+F_4)$

$F_1=h^3+\varepsilon^*+3h^2\alpha^*+3h(\alpha^{*2}+\sigma^{*2})+3\alpha^*\sigma^{*2}+\alpha^{*3}+12l^2(h+\alpha^*)$,

$F_2=-6Nl(h^2+\alpha^{*2}+\sigma^{*2}+2h\alpha^*)$,

$F_3=\left\{1-\cot h^2(Nh/2l)\right\}\left\{\frac{N\alpha}{2l}-\frac{N^3}{24l^3}\right\}\left(\varepsilon^*+\alpha^{*3}+3\alpha^*\sigma^{*2}\right)$ and

$F_4=\cot h\ (Nh/2l)\left\{1-\frac{N^2}{4l^2}(\alpha^{*2}+\sigma^{*2})\right\}$. $\frac{\partial H}{\partial t}=c\frac{d\varepsilon}{dt}\cos\theta$

Introducing the non-dimensional scheme into equation (19)

$\theta=\frac{x}{R}$, $\bar{z}=\frac{z}{L}$, $\bar{l}=\frac{l}{c}$, $\bar{H}=\frac{H}{c}=\bar{h}+\bar{h}_s$, $\bar{h}=\frac{h}{c}=1+\varepsilon\cos\theta$, $\bar{h}_s=\frac{h_s}{c}$ $\bar{k}=\frac{k}{c^2}$, $\bar{H}_0=\frac{H_0}{c}$, $\bar{x}=\frac{x}{R}$, $\bar{\alpha}=\frac{\alpha^*}{c}$,

$\sigma^2=\frac{\sigma^{*2}}{c^2}$, $\varepsilon_1=\frac{\varepsilon^*}{c^3}$, $\lambda=\frac{L}{2R}$, $\psi=\frac{kH_0}{c^3}$

$\bar{p}=\frac{E(p)c^2}{\mu R^3\left(\frac{d\varepsilon}{dt}\right)}$, $N=\left(\frac{\chi}{\chi+2\mu}\right)^{\frac{1}{2}}$.

The modified Reynolds equation (17) can be written in a non- dimensional form as

$$\frac{\partial}{\partial\theta}\left\{E\left[\bar{f}(N,\bar{l},\bar{H})+12\psi\left(\frac{1-N^2}{1+N^2}\right)\right]\frac{\partial E(\bar{p})}{\partial\theta}\right\}+\left(\frac{1}{4\lambda^2}\right)\frac{\partial}{\partial\bar{z}}\left\{E\left[\bar{f}(N,\bar{l},\bar{H})+12\psi\left(\frac{1-N^2}{1+N^2}\right)\right]\frac{\partial E(\bar{p})}{\partial\bar{z}}\right\}=12\cos\theta \quad (18)$$

where $\bar{f}(N,\bar{l},\bar{H})=\bar{H}^3+12\bar{l}^2\bar{H}-6N\bar{l}\bar{H}^2\coth\left(\frac{N\bar{H}}{2\bar{l}}\right)$.

As the permeability parameter $\psi\to 0$, equation (18) reduces to the corresponding solid case. For the 180^0 partial porous journal bearing, the boundary conditions for the fluid film pressure are

$$\bar{p}=0 \quad \text{at} \quad \theta=\frac{\pi}{2},\frac{3\pi}{2} \quad \text{and} \quad \bar{p}=0 \quad \text{at} \quad \bar{z}=\pm\frac{1}{2} \quad (19)$$

The modified Reynolds equation will be solved numerically by using a finite difference scheme. The film domain under consideration is divided by grid spacing shown in figure2. In finite increment format, the terms of equation (18) can be expressed as

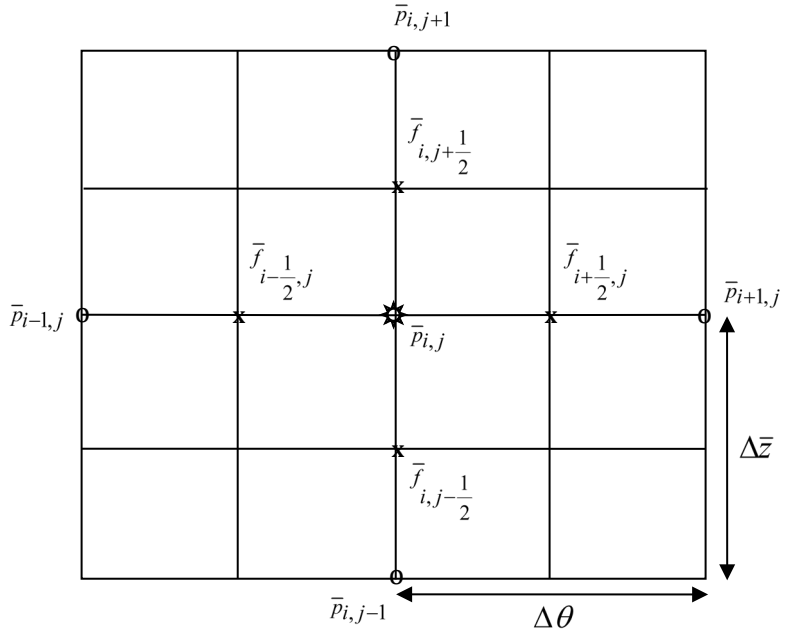

Fig. 2. Grid point notation for film domain

$$\frac{\partial}{\partial\theta}\left[\left\{\bar{f}+12\psi\left(\frac{1-N^2}{1+N^2}\right)\right\}\frac{\partial\bar{P}}{\partial\theta}\right]=$$

$$\frac{1}{\Delta\theta}\left[\left(\bar{f}_{i+\frac{1}{2},j}+12\psi\left(\frac{1-N^2}{1+N^2}\right)\right)\left(\frac{\bar{P}_{i+1,j}-\bar{P}_{i,j}}{\Delta\theta}\right)-\left(\bar{f}_{i-\frac{1}{2},j}+12\psi\left(\frac{1-N^2}{1+N^2}\right)\right)\left(\frac{\bar{P}_{i,j}-\bar{P}_{i-1,j}}{\Delta\theta}\right)\right] \quad (20)$$

$$\frac{1}{4\lambda^2}\times\frac{\partial}{\partial\bar{z}}\left[\left\{\bar{f}+12\psi\left(\frac{1-N^2}{1+N^2}\right)\right\}\frac{\partial\bar{P}}{\partial\bar{z}}\right]=$$

$$\frac{1}{4\lambda^2}\times\frac{1}{\Delta\bar{z}}\left[\left(\bar{f}_{i,j+\frac{1}{2}}+12\psi\left(\frac{1-N^2}{1+N^2}\right)\right)\left(\frac{\bar{P}_{i,j+1}-\bar{P}_{i,j}}{\Delta\bar{z}}\right)-\left(\bar{f}_{i,j-\frac{1}{2}}+12\psi\left(\frac{1-N^2}{1+N^2}\right)\right)\left(\frac{\bar{P}_{i,j}-\bar{P}_{i,j-1}}{\Delta\bar{z}}\right)\right] \quad (21)$$

Substituting these expressions (20) and (21) into the Reynolds equation (20) we get

$$\bar{P}_{i,j}=C_1\bar{P}_{i+1,j}+C_2\bar{P}_{i-1,j}+C_3\bar{P}_{i,j+1}+C_4\bar{P}_{i,j-1}+C_5 \quad (22)$$

where

$$C_0 = 4\lambda^2 r^2 \left\{ \left(\bar{f}_{i+1/2,j} + 12\psi \left(\frac{1-N^2}{1+N^2} \right) \right) + \left(\bar{f}_{i-1/2,j} + 12\psi \left(\frac{1-N^2}{1+N^2} \right) \right) \right\}$$
$$+ \left(\bar{f}_{i,j+1/2} + 12\psi \left(\frac{1-N^2}{1+N^2} \right) \right) + \left(\bar{f}_{i,j-1/2} + 12\psi \left(\frac{1-N^2}{1+N^2} \right) \right)$$

$$C_1 = 4\lambda^2 r^2 \left(\bar{f}_{i+1/2,j} + 12\psi \left(\frac{1-N^2}{1+N^2} \right) \right) \Big/ C_0 ,$$

$$C_2 = 4\lambda^2 r^2 \left(\bar{f}_{i-1/2,j} + 12\psi \left(\frac{1-N^2}{1+N^2} \right) \right) \Big/ C_0 ,$$

$$C_3 = \left(\bar{f}_{i,j+1/2} + 12\psi \left(\frac{1-N^2}{1+N^2} \right) \right) \Big/ C_0 ,$$

$$C_4 = \left(\bar{f}_{i,j-1/2} + 12\psi \left(\frac{1-N^2}{1+N^2} \right) \right) \Big/ C_0 ,$$

$$C_5 = -48\lambda^2 \cos\theta_i \Delta\bar{z}^2 \Big/ C_0 , \; r = \frac{\Delta\bar{z}}{\Delta\theta}.$$

The pressure, $\bar{p}$ is calculated by using the numerical method with grid spacing of $\Delta\theta = 9^0$ and $\Delta\bar{z} = 0.05$.

The load carrying capacity of the bearing, $W(t)$ generated by the film pressure is obtained by

$$E(W(t)) = -LR \int_{\theta=\pi/2}^{\theta=3\pi/2} \int_{z=-1/2}^{z=1/2} p \cos\theta \, d\theta . dz \qquad (23)$$

For the bearing operating under steady load, $W(s)$ the generated load, $W(t)$ due to the squeeze film equals the applied load, $W(s)$

$$E(W(t)) = E(W(s)) \qquad (24)$$

Using equations (22) and (24) in equation (23) the non-dimensional load carrying capacity, $\bar{W}$ is obtained in the form

$$\bar{W} = \frac{E(W(s))c^2}{\mu LR^3 \left(\frac{d\varepsilon}{dt} \right)} = - \int_{\theta=\pi/2}^{\theta=3\pi/2} \int_{\bar{z}=-1/2}^{\bar{z}=1/2} \bar{P}_{i,j} \cos\theta_i d\theta . d\bar{z} \qquad (25)$$

$$\approx \sum_{i=0}^{M} \sum_{j=0}^{N} \bar{P}_{i,j} \cos\theta_i \Delta\theta . \Delta\bar{z} = g\left(\varepsilon, \bar{l}, N, \psi, \alpha, \sigma, \varepsilon_1 \right) \qquad (26)$$

where M+1 and N+1 are the grid point numbers in the x and z directions respectively.

In many practical applications, the squeeze film journal bearings operate under dynamic conditions. Under such conditions, the path of the rotor centre fluctuates in a manner compatible to the variations in the applied load. To simulate this type of situation , the applied load is considered as a sinusoidal function of time.

$$E(W(t)) = W_0 \sin(\omega t) \qquad (27)$$

Where W_0 is the amplitude and ω is the frequency of the applied load oscillations. Using equations (26) and (27) in equation (25) the velocity of the journal centre is obtained as

$$\frac{d\varepsilon}{d\tau} = \frac{60\sin\tau}{S\pi g\left(\varepsilon, \bar{l}, N, \psi, \alpha, \sigma, \varepsilon_1\right)} \tag{28}$$

Where $S = \dfrac{\mu N}{\left(W0/2LR\right)}\left(\dfrac{R}{C}\right)^2$ is the Sommerfeld number and

$\tau = \omega t = \left(\dfrac{2\pi N}{60}t\right)$ is the dimensionaless response time.

4. RESULTS AND DISCUSSIONS

To solve squeeze film pressure in the equation (22) the mesh of the film domain has 20 equal intervals along the bearing length and circumference. The co-efficient matrix of the system of algebraic equations is of pentadiagonal form. These equations have been solved by using Scilab tools.

The effect on the static and dynamic behaviors of squeeze film in finite rough porous journal bearings has been studied on the basis of Eringen [ ] microcontinuum theory for micropolar fluids.

The squeeze film lubrication characteristic of a finite rough porous journal bearings lubricated with micropolar fluids are obtained on the basis of various non-dimensional parameters such as the coupling number, $N\left(=\dfrac{\chi}{\chi+2\mu}\right)^{1/2}$ which characterizes the coupling between the Newtonian and microrotational viscosities, the parameter, $\bar{l}\left(=l/c\right)$ in which $\bar{l}$ has the dimension of length and may be considered as chain length of microstructures additives. The parameter $\bar{l}$, characterizes the interaction of the bearing geometry with the lubricant properties. In the limiting case as $\bar{l} \to 0$ the effect of microstructures becomes negligible. The effect of permeability is observed through the non-dimensional permeability parameter, $\psi\left(=\dfrac{kH_0}{c^3}\right)$ and it is to be noted that as $\psi \to 0$ the problem reduces to the corresponding solid case and as $\bar{l}, N \to 0$ it reduces to the corresponding Newtonian case. The non-dimensional parameters α, ε_1 and σ characterizes the type of roughness asperities on the bearing surface. The values of these parameters are so choosen that the corresponding film shapes be feasible. The static and dynamic squeeze film characteristics for finite rough porous journal bearings with no journal rotation have been computed by using equation (22), (26) and (28) and are presented in figures 3 to 23.

4.1. SQUEEZE FILM PRESSURE

The effect of Micropolarity on the variations of non-dimensional squeeze film pressure $\bar{p}$ with the circumferential co-ordinate θ for different values of $\bar{l}$ and *N* is depicted in the fig .3 and 4. It is observed that $\bar{p}$ increases significantly for increasing values of $\bar{l}$ and *N*. The effect of roughness parameters α, ε_1 and σ on the variation of $\bar{p}$ with θ is depicted in the Figs 5 to 7. it is observed that $\bar{p}$ increases for negatively increasing values α and ε_1, where as positively increasing values of α and ε_1 decreases $\bar{p}$ (Figs 5 and 6). The increasing values of σ decreases $\bar{p}$ significantly. The effect of permeability ψ on the variation of $\bar{p}$ is shown in fig.8. It is observed that the increasing values of permeability parameter ψ decreases $\bar{p}$.

4.2. LOAD CARRYING CAPACITY

The variation of non-dimensional mean load carrying capacity $\bar{W}$ with the eccentricity ratio parameter, ε for different values of $\bar{l}$ and two values of the permeability parameter, $\psi = 0.1, 0.01$ is depicted in the figure 9. it is observed that the increasing values of $\bar{l}$ increases $\bar{W}$ as compared to corresponding Newtonian case $\left(\bar{l} \to 0\right)$. The variation of non-dimensional load carrying capacity $\bar{W}$ with the eccentricity ratio parameter, ε for different value of N and two values of the permeability parameter, $\psi = 0.1, 0.01$ is depicted in the figure.10. It is observed that the increasing values of N increases $\bar{W}$ for both the values of ψ.

The effect of roughness parameters α, ε_1 and σ on the variation of $\bar{W}$ with the eccentricity ratio parameter, ε is depicted in Figs 11 to 13. it is observed that the negatively skewed surface roughness increases $\bar{W}$, where as the positively skewed surface roughness decreases $\bar{W}$ (Figs 11 and 12). Further, it is observed that $\bar{W}$ decreases for increasing values of σ.

4.3. JOURNAL CENTRE VELOCITY

The effect of micropolar parameters $\bar{l}$ and N on the variation of the journal centre, $\left(\frac{d\varepsilon}{dt}\right)$ with non-dimensional time parameter τ is depicted in the fig. 14 and 15 respectively and two values of permeability parameter ψ. It is observed that the journal bearing lubricated with micropolar fluid experiences high resistance to be motion of the journal centre as compared to the Newtonian case. This is an encouraging result for the lubrication engineers, because it implies that the journal centre will take a longer time to come in contact with the bearing surface which in term increases the bearing life. The effect of the roughness parameters α, ε_1 and σ on variations of $\left(\frac{d\varepsilon}{dt}\right)$ with non-dimensional time parameter τ is depicted in the fig. 16 and 18, respectively. It is interesting to note that negatively skewed surface roughness on the bearing surface experience more resistance to the motion of the journal centre, where as the positively skewed surface roughness causes the increases in the journal centre velocity.

4.4. LOCUS OF THE JOURNAL CENTRE

The locus of the journal centre, ε is obtained by solving the equation (28) with an initial condition, $\varepsilon(0) = 0.0$. It is observed from Figs 19 and 20, that the rough journal bearing lubricated with micropolar fluids operates with lesser eccentricity ratio ε than that with Newtonian lubricant. It is due to the fact that, the micropolar fluids offer greater resistance to the journal motion. Therefore, the same load can be applied for a longer time period for the journal bearings with micropolar fluids as lubricant.

These effects are more pronounced for the journal bearing with negatively skewed surface roughness on the bearing surface (figs 21 and 22). Fig.23 Shows the variation of ε with τ for different values of σ. It is observed that ε increases for increasing values of σ.

5. CONCLUSIONS

On the basis of Eringen [1] micropolar fluid theory and general stochastic method for the study of surface roughness, this paper predicts the effect of surface roughness on the static and dynamic characteristics of pure squeeze film lubrication of finite porous journal bearing with no journal rotations lubricated with micropolar fluids. The film pressure distribution is solved numerically by using finite difference technique with a grid spacing of $\Delta\theta = 9^0$ and $\Delta\bar{z} = 0.05$. On the basis of the results computed the following conclusions are drawn below.

1) The presence of microstructure additives in the lubricant provides an enhancement in the fluid film pressure and the load carrying capacity whereas the journal center velocity reduces.
2) The micropolar fluids offer the more resistance to the journal motion and hence the same load can be applied for longer period of time for the journal bearings with micropolar fluids as compared to the corresponding Newtonian lubricant.
3) The positively skewed surface roughness on the bearing surface increases the fluid film pressure, load carrying capacity and decreases the journal center velocity hence the life of the journal bearing can be improved due to the presence of negatively skewed surface roughness on the bearing surfaces.
4) The presence of positively skewed surface roughness on the bearing surface adversely affects the performance of the journal bearing.

CONFLICT OF INTERESTS

None.

ACKNOWLEDGMENTS

None.

REFERENCES

Eringen AC. Theory of micropolar fluids. J. Mathematics and mechanics 1966; 16:1-18.
Eringen AC. Simple microfluids. Int. J. Engng Science, 1964 ; 2 :205-217.
Zaheeruddin KH, Isa M. Micropolar fluid lubrication of one-dimensional journal bearing. Wear 1978; 50: 211-220.
Huang TW. Analysis of finite width journal bearing with micropolar fluids. Wear 1988; 123:1-12.
Khonasari MM, Brewe D. On the performance of finite journal bearings lubricated with micropolar fluid. Tribology Tran 1989; 32(2):155-160.
Ramanaiah G, Dubey JN. Optimum slider profile of a slider bearing lubricated with a micropolar fluid. Wear 1977; 76:199-209.
Naduvinamani NB, Siddangouda A. on the performance of rough inclined Stepped composite bearings with micropolar fluid. J. of Marine Science & Tech. 2010; 18(2): 233-242.
Bujurke NM, Bhavi SG, Hiremath PS. Squeeze film lubricated with micropolar fluids. Proc. Indian natn. Sci. acad 1987;53 A: 391-398.
Agrawal VK, Ganju KL, Jethi SC. Squeeze film and externally pressurized bearings lubricated with micropolar fluid. Wear 1972; 19:259-265.
Balaram M, Micropolar squeeze film. J. Lubri. Tech.1975; 635-637.
Prakash J, Sinha P. Cyclic squeeze films in micropolar fluid lubricated journal bearings. Trans ASME. J .Lubri. Technol. 1975;98 : 412-417.
Sinha P. Dynamically loaded micropolar fluid lubricated journal bearings with special reference to the squeeze films under fluctuating loads. Wear 1977; 45: 279-292.
Isa M, Zaheeruddin K. One dimensional porous journal bearing lubricated with micropolar fluid. Wear 1978; 50(2): 211-220.
Verma PDS, Agrawal VK, Bhat SB. Porous inclined slider bearing lubricated with micropolar fluid. Wear 1979; 53:101-106.
Naduvinamani NB, Huggi SS. Micropolar fluid squeeze film lubrication of short partial porous journal bearing. J. Engg. Tribol. 2009; (223): 1179-1185.
Christensen H. Stochastic models for hydrodynamic lubrication of rough surfaces. Proc. of Instn. Mech. Engrs. Part I 1969-1970; 184:1013-1026.

Christensen H, Tonder K. The hydrodynamic lubrication of rough bearing surfaces of finite width. ASME J. Lubri. Tech. 1971; 93: 324-330.
Prakash J, Tiwari K. An analysis of squeeze film between porous rectangular plates including the surface roughness effects. Journal of Mechanical Engineering Science. 1982b; 24(1): 45-49.
Prakash J, Tiwari K. Effects of surface roughness on the squeeze film between rotating porous annular discs. Journal of Mechanical Engineering Science. 1982c; 24(3): 155-161.
Gururajan K, Prakash J. surface roughness effects in infinitely long porous journal bearings. ASME Journal of Tribology, 1999; 121: 139-147.
Gururajan K, Prakash J. Effects of surface roughness in a narrow porous journal bearing, ASME Journal of Tribology, 2000; 122: 472-475.
Naduvinamani NB, Kashinath B. Surface roughness effecte on the static and dynamic behaviour of squeeze film lubrication of short journal bearings with micropolar fluids. J. Engg. Tribol.2008; 222: 1-11.
Naduvinamani NB, Santosh S. On the squeeze film lubrication of rough short porous partial journal bearings with micropolar fluid. J. Engg. Tribol. 2009;224: 249-257 .
Andharia PI. Gupta JL., Deheri GM. Effect of surface roughness on hydrodynamic lubrication of slider bearings. Tribol Trans. 2001; 44(2): 291- 297.
Verma PDS, Agrawal VK, Bhat SK. Porous inclined slider bearing lubricated with micropolar fluid. Wear 1979 ;53: 101-106.

Fig 1: Physical configuration of a finite rough porous journal bearing.

Fig 2: Grid point notation for film domain.

Fig 3: The variation of Non-dimensional film pressure $\overline{p}$ with circumferential co-ordinate θ for different values of $\overline{l}$ with $N = 0.6, \psi = 0.1, \overline{\alpha} = 0.1$, $\overline{\sigma} = 0.15, \overline{\varepsilon}_1 = 0.1, \lambda = 0.75 \; and \; \varepsilon = 0.2$

Fig 4: The variation of Non-dimensional film pressure $\overline{p}$ with circumferential co-ordinate θ for different values of N with $\overline{l} = 0.2, \psi = 0.1, \overline{\alpha} = 0.1$, $\overline{\sigma} = 0.15, \overline{\varepsilon}_1 = 0.1, \lambda = 0.75 \; and \; \varepsilon = 0.2$

Fig 5: The variation of Non-dimensional film pressure $\overline{p}$ with circumferential co-ordinate θ for different values of $\overline{\alpha}$ with $\overline{l} = 0.2, \psi = 0.1, N = 0.6$, $\overline{\sigma} = 0.15, \overline{\varepsilon}_1 = 0.1, \lambda = 0.75 \; and \; \varepsilon = 0.2$

Fig 6: The variation of Non-dimensional film pressure $\bar{p}$ with circumferential co-ordinate θ for different values of $\bar{\varepsilon}_1$ with $\bar{l} = 0.2, \psi = 0.1, N = 0.6$, $\bar{\alpha} = 0.1, \bar{\sigma} = 0.15, \lambda = 0.75 \; and \; \varepsilon = 0.2$

Fig 7: The variation of Non-dimensional film pressure $\bar{p}$ with circumferential co-ordinate θ for different values of $\bar{\sigma}$ with $\bar{l} = 0.2, \psi = 0.1, N = 0.6$, $\bar{\alpha} = 0.1, \bar{\varepsilon}_1 = 0.1, \lambda = 0.75 \; and \; \varepsilon = 0.2$

Fig 8: The variation of Non-dimensional film pressure $\bar{p}$ with circumferential co-ordinate θ for different values of ψ with $\bar{l} = 0.2, \; N = 0.6, \bar{\alpha} = 0.1$, $\bar{\sigma} = 0.15, \bar{\varepsilon}_1 = 0.1, \lambda = 0.75 \; and \; \varepsilon = 0.2$

Fig 9: Variation of Non-dimensional load $\bar{W}$ with ε for different values of $\bar{l}$ with $N = 0.6, \psi = 0.1, \bar{\alpha} = 0.1, \bar{\sigma} = 0.15, \bar{\varepsilon}_1 = 0.1 \; and \; \lambda = 0.75$.

Fig 10: Variation of Non-dimensional load $\bar{W}$ with ε for different values of N with $\bar{l} = 0.2, \psi = 0.1, \bar{\alpha} = 0.1, \bar{\sigma} = 0.15, \bar{\varepsilon}_1 = 0.1 \; and \; \lambda = 0.75$.

Fig 11: Variation of Non-dimensional load $\bar{W}$ with ε for different values of $\bar{\alpha}$ with $N = 0.6, \bar{l} = 0.2, \psi = 0.1, \; \bar{\sigma} = 0.15, \bar{\varepsilon}_1 = 0.1 \; and \; \lambda = 0.75$.

Fig 12: Variation of Non-dimensional load $\bar{W}$ with ε for different values of $\bar{\varepsilon}_1$ with $N = 0.6, \bar{l} = 0.2, \psi = 0.1, \bar{\alpha} = 0.1, \; \bar{\sigma} = 0.15 and \; \lambda = 0.75$.

Fig 13: Variation of Non-dimensional load $\bar{W}$ with ε for different values of $\bar{\sigma}$ with $N = 0.6, \bar{l} = 0.2, \psi = 0.1, \; \bar{\alpha} = 0.1, \bar{\varepsilon}_1 = 0.1 \; and \; \lambda = 0.75$.

Fig 14: Velocity of the journal centre, $\left(\frac{d\varepsilon}{dt}\right)$ verses τ for different values of $\bar{l}$ with

$N = 0.6, \bar{\alpha} = 0.1, \bar{\sigma} = 0.15, \bar{\varepsilon}_1 = 0.1, \lambda = 0.75, \varepsilon = 0.2 \; and s = 0.9$.

Fig 15: Velocity of the journal centre, $\left(\frac{d\varepsilon}{dt}\right)$ verses τ for different values of N with

$\bar{l} = 0.2, \bar{\alpha} = 0.1, \bar{\sigma} = 0.15, \bar{\varepsilon}_1 = 0.1, \lambda = 0.75, \varepsilon = 0.2 \; and s = 0.9$.

Fig 16: Velocity of the journal centre, $\left(\frac{d\varepsilon}{dt}\right)$ verses τ for different values of $\bar{\alpha}$ with

$N = 0.6, \bar{l} = 0.2, \psi = 0.1, \bar{\sigma} = 0.15, \bar{\varepsilon}_1 = 0.1, \lambda = 0.75, \varepsilon = 0.2 \; and \; s = 0.9$.

Fig 17: Velocity of the journal centre, $\left(\frac{d\varepsilon}{dt}\right)$ verses τ for different values of $\bar{\varepsilon}_1$ with

$N = 0.6, \bar{l} = 0.2, \psi = 0.1, \bar{\sigma} = 0.15, \bar{\alpha} = 0.1, \lambda = 0.75, \varepsilon = 0.2 \; and \; s = 0.9$.

Fig 18: Velocity of the journal centre, $\left(\frac{d\varepsilon}{dt}\right)$ verses τ for different values of $\bar{\sigma}$ with

$N = 0.6, \bar{l} = 0.2, \psi = 0.1, \bar{\alpha} = 0.1, \bar{\varepsilon}_1 = 0.1, \lambda = 0.75, \varepsilon = 0.2 \; and \; s = 0.9$.

Fig 19: Variation of locus of the journal centre ε verses τ for different values of

$\bar{l}$ with $N = 0.6, \bar{\alpha} = 0.1, \bar{\sigma} = 0.15, \bar{\varepsilon}_1 = 0.1, \lambda = 0.75, \varepsilon = 0.2 and \; s = 0.9$

Fig 20: Variation of locus of the journal centre ε verses τ for different values of

N with $\bar{l} = 0.2, \bar{\alpha} = 0.1, \bar{\sigma} = 0.15, \bar{\varepsilon}_1 = 0.1, \lambda = 0.75, \varepsilon = 0.2 and \; s = 0.9$

Fig 21: Variation of locus of the journal centre ε verses τ for different values of

$\bar{\alpha}$ with $N = 0.6, \bar{l} = 0.2, \psi = 0.1, \bar{\sigma} = 0.15, \bar{\varepsilon}_1 = 0.1, \lambda = 0.75, \varepsilon = 0.2 and \; s = 0.9$

Fig 22: Variation of locus of the journal centre ε verses τ for different values of

$\bar{\varepsilon}_1$ with $N = 0.6, \bar{l} = 0.2, \psi = 0.1, \bar{\sigma} = 0.15, \bar{\alpha} = 0.1, \lambda = 0.75, \varepsilon = 0.2 and \; s = 0.9$

Fig 23: Variation of locus of the journal centre ε verses τ for different values of

$\bar{\sigma}$ with $N = 0.6, \bar{l} = 0.2, \psi = 0.1, \bar{\alpha} = 0.1, \bar{\varepsilon}_1 = 0.1, \lambda = 0.75, \varepsilon = 0.2 and \; s = 0.9$

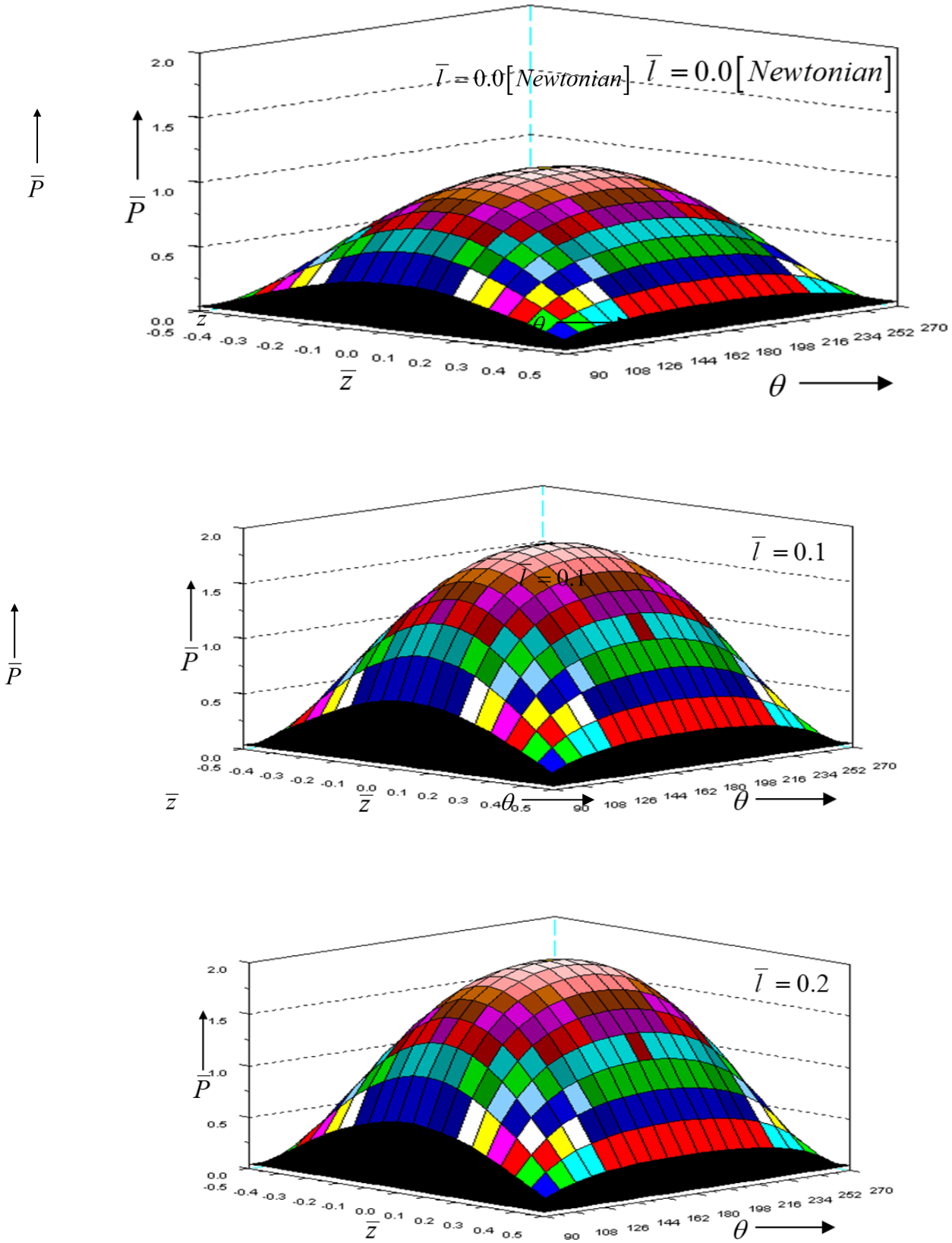

Figure 3. The Variation of non-dimensional film pressure with circumferential co-ordinate for different values of with and

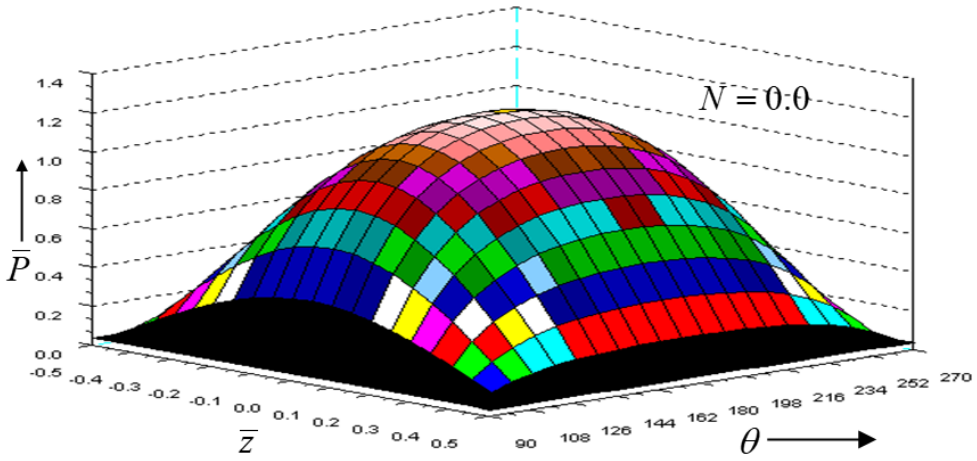
N = 0.0
$\overline{P}$
1.4
1.2
1.0
0.8
0.6
0.4
0.2
0.0
-0.5 -0.4 -0.3 -0.2 -0.1 0.0 0.1 0.2 0.3 0.4 0.5
$\overline{z}$
90 108 126 144 162 180 198 216 234 252 270
θ

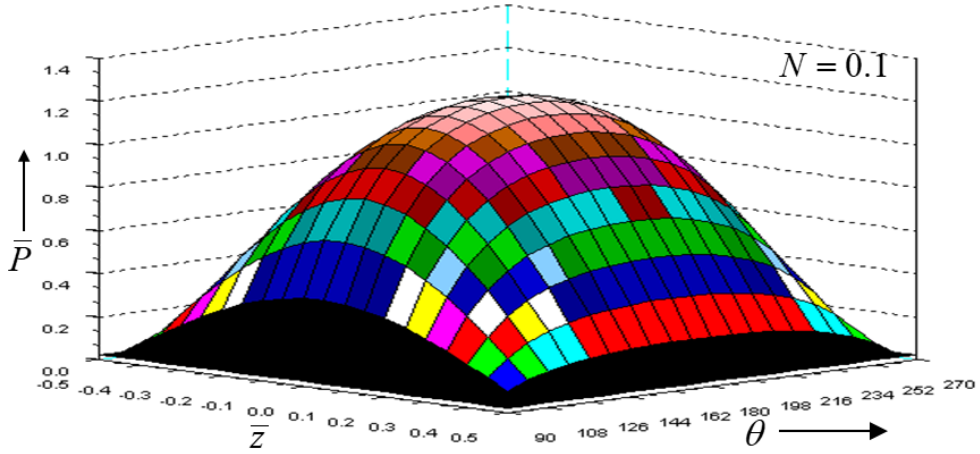
N = 0.1
$\overline{P}$
1.4
1.2
1.0
0.8
0.6
0.4
0.2
0.0
-0.5 -0.4 -0.3 -0.2 -0.1 0.0 0.1 0.2 0.3 0.4 0.5
$\overline{z}$
90 108 126 144 162 180 198 216 234 252 270
θ

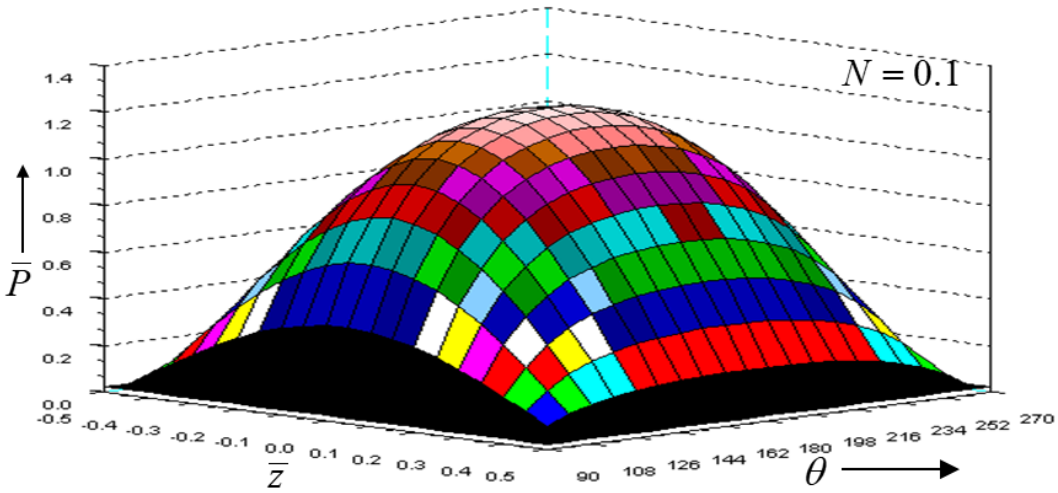
N = 0.1
$\overline{P}$
1.4
1.2
1.0
0.8
0.6
0.4
0.2
0.0
-0.5 -0.4 -0.3 -0.2 -0.1 0.0 0.1 0.2 0.3 0.4 0.5
$\overline{z}$
90 108 126 144 162 180 198 216 234 252 270
θ

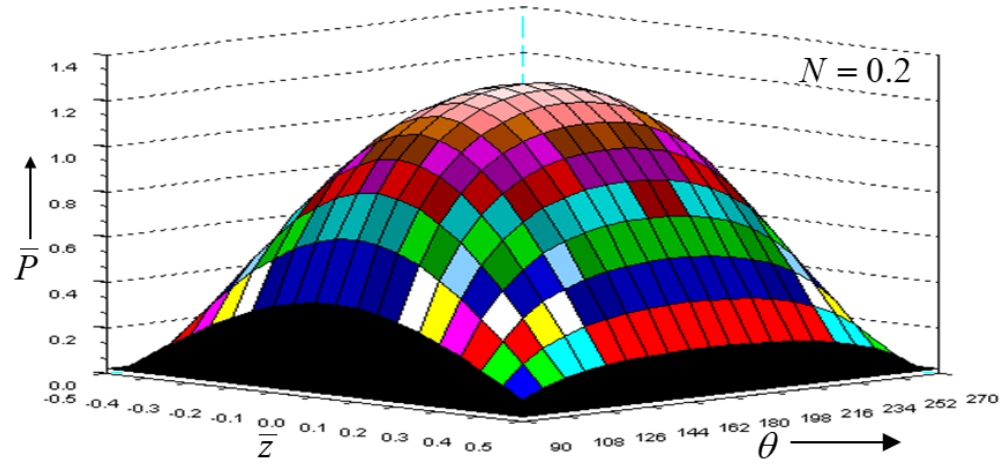

Figure 4. The Variation of non-dimensional film pressure with circumferential co-ordinate for different values of with and $\varepsilon = 0.2$

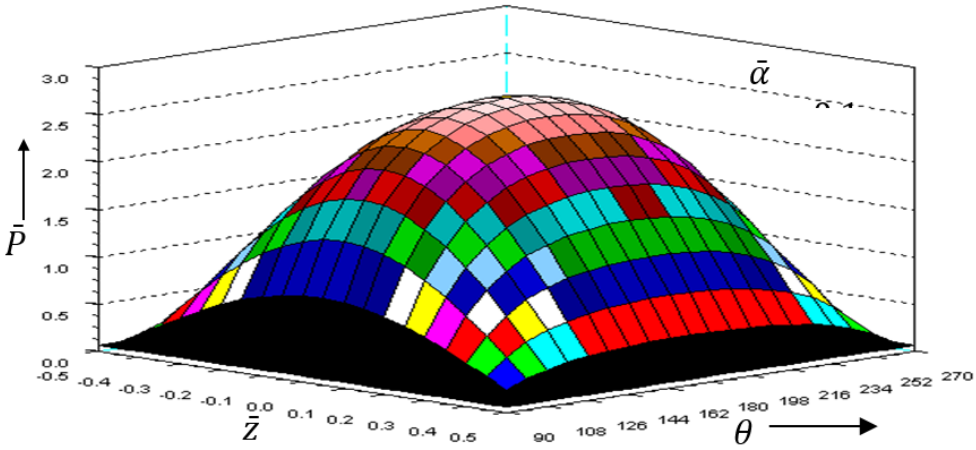

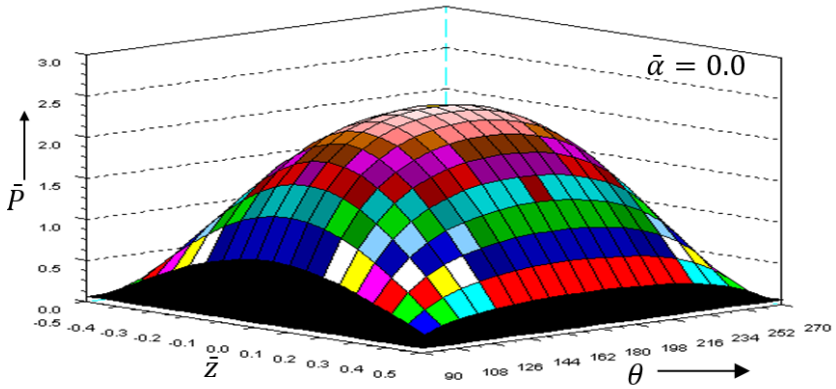

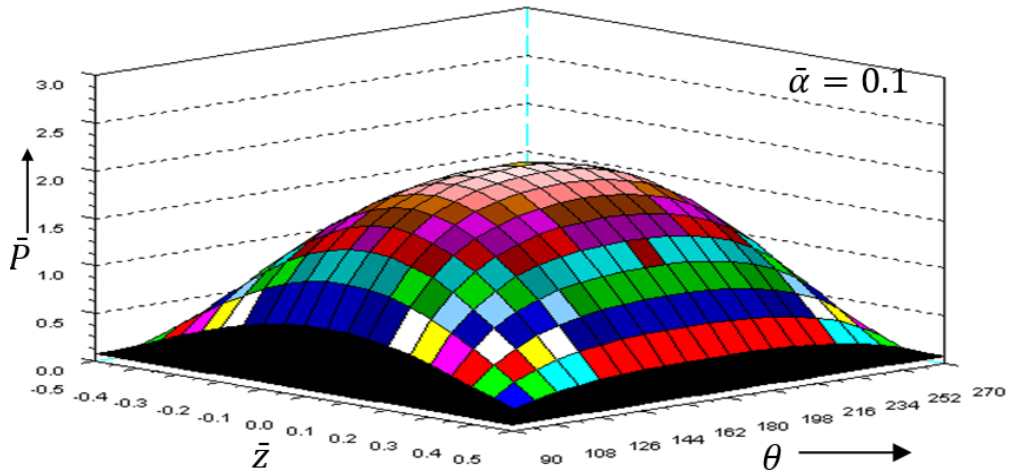

Figure 5. The Variation of non-dimensional film pressure with circumferential co-ordinate for different values of αwith N=0.6,Γ=0.2,ψ=0.1,σ¯=0.15,ε¯_1=0.1,λ=0.75and ε=0.2

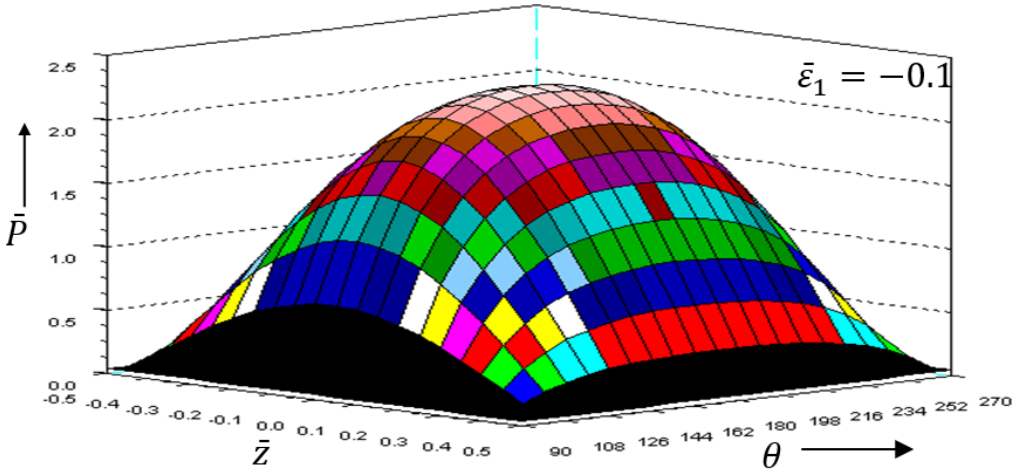

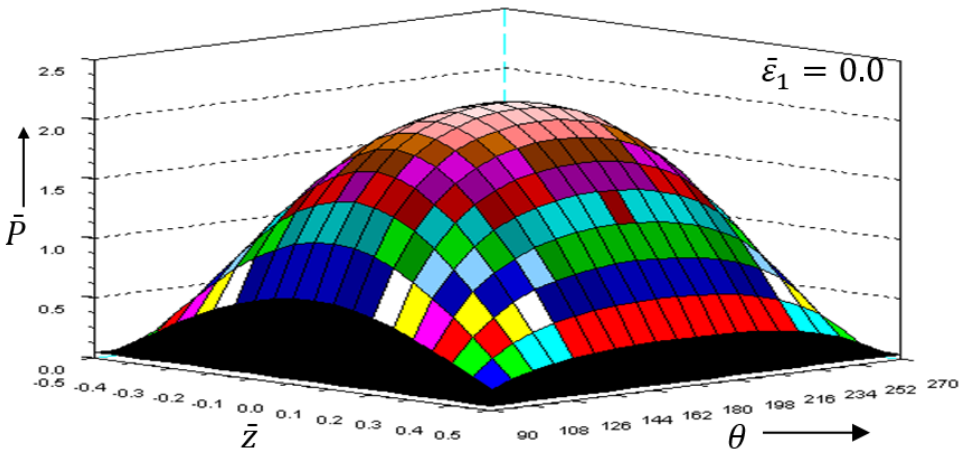

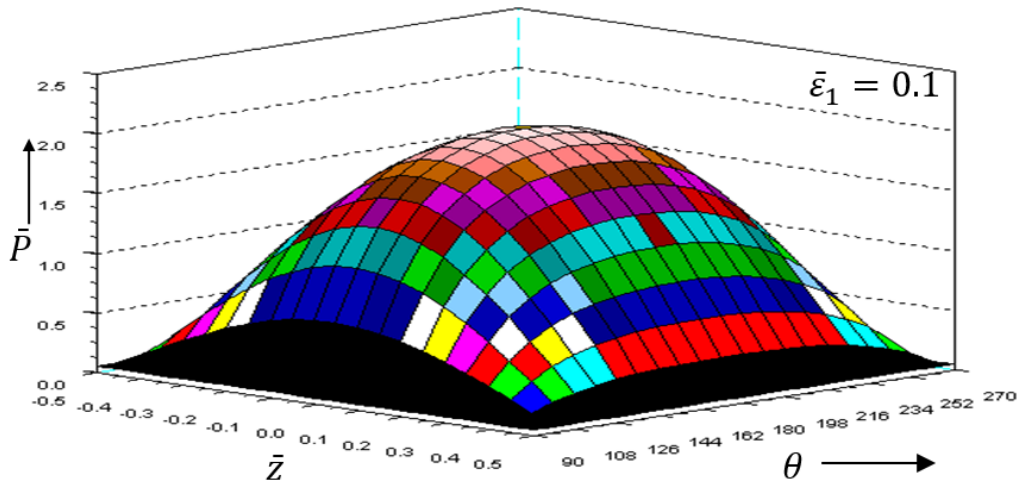

Figure 6 The Variation of non-dimensional film pressure with circumferential co-ordinate for different values of ε¯_1with N=0.6,Γ¯=0.2,ψ=0.1,α¯=0.1,σ¯=0.15,λ=0.75and ε=0.2

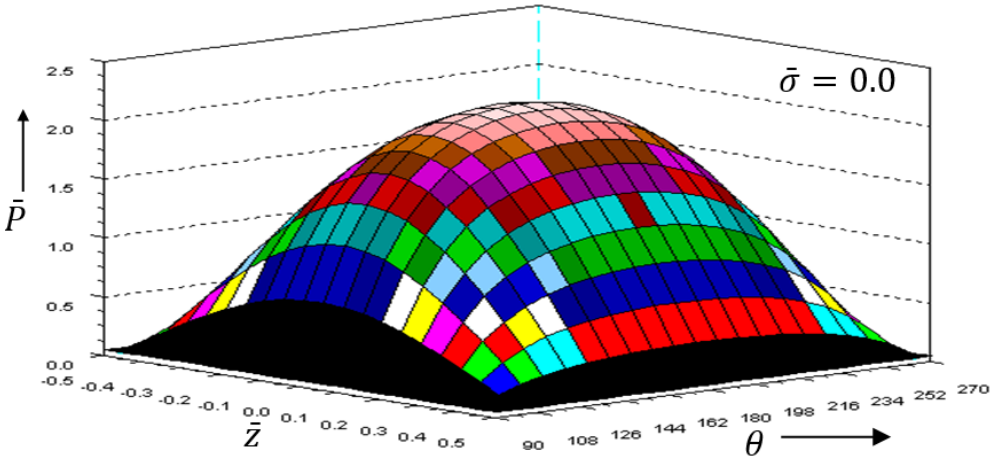

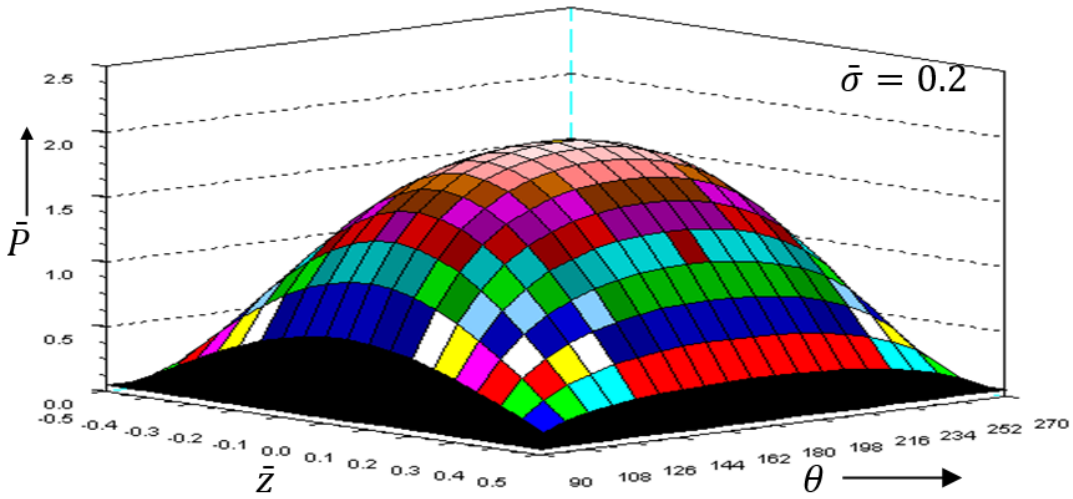

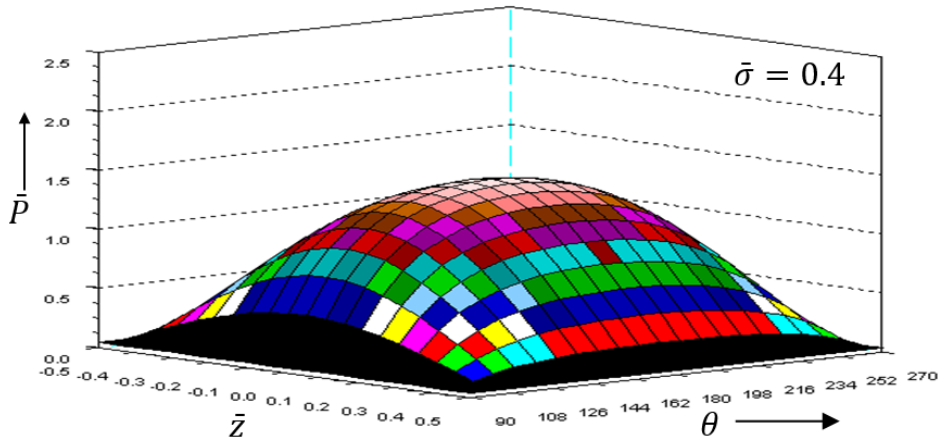

Figure 7. The Variation of non-dimensional film pressure with circumferential co-ordinate for different values of σ¯with N=0.6,Γ¯=0.2,ψ=0.1,α¯=0.1,ε¯_1=0.1,λ=0.75and ε=0.2

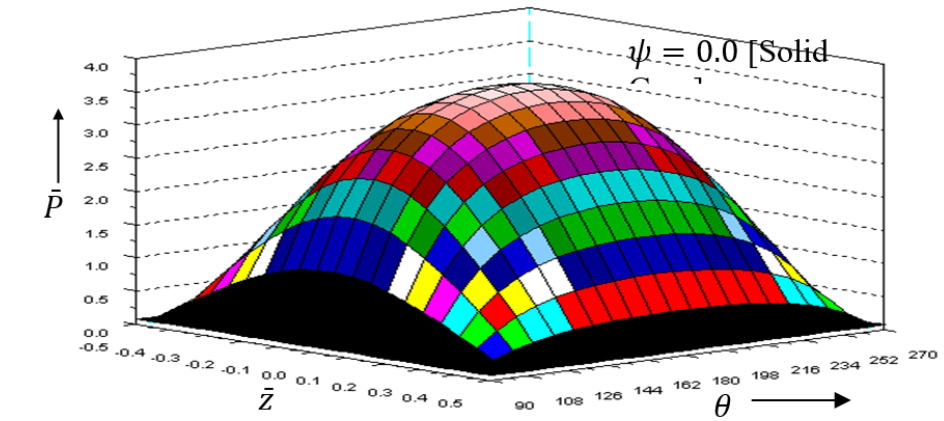

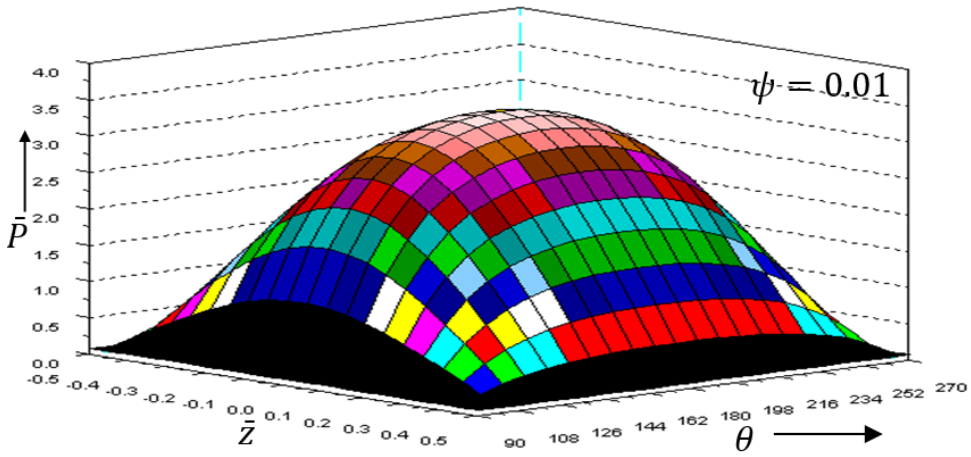

Fig.8. The Variation of non-dimensional film pressure with circumferential co-ordinate for different values of ψwith N=0.6,Γ¯=0.2,α¯=0.1,σ¯=0.15,ε¯_1=0.1,λ=0.75and ε=0.2

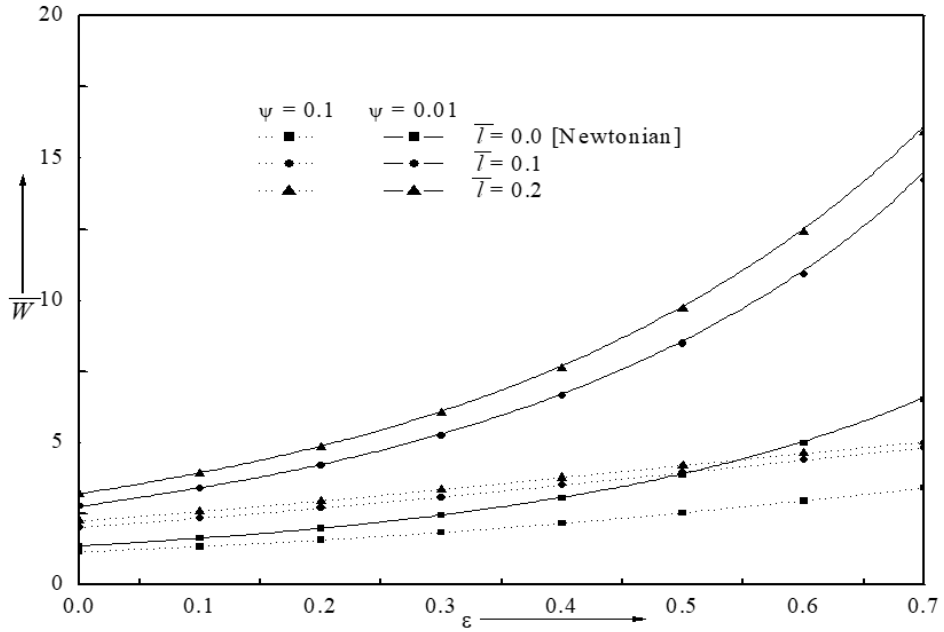

Fig.9. Variation of non-dimensional load $\overline{W}$ with ε for different values of $\overline{l}$ with N = 0.6, ψ = 0.1, $\overline{\alpha}$ = 0.1, $\overline{\sigma}$ = 0.15, $\overline{\varepsilon_1}$ = 0.1 and λ = 0.75

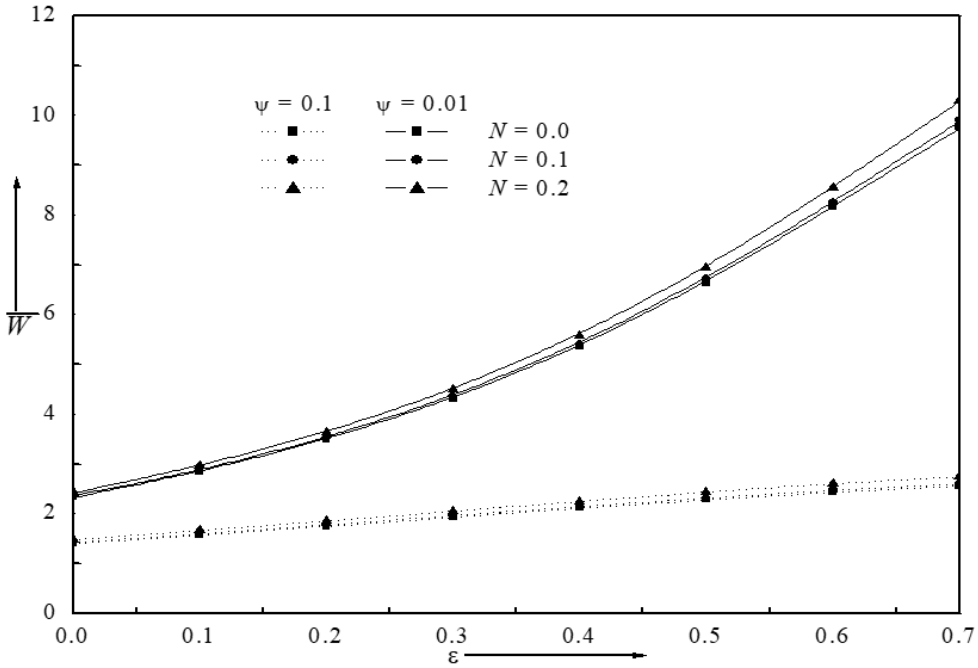

Fig.10. Variation of non-dimensional load $\overline{W}$ with ε for different values of N with $\overline{l}$ = 0.2, ψ = 0.1, $\overline{\alpha}$ = 0.1, $\overline{\sigma}$ = 0.15, $\overline{\varepsilon_1}$ = 0.1 and λ = 0.75

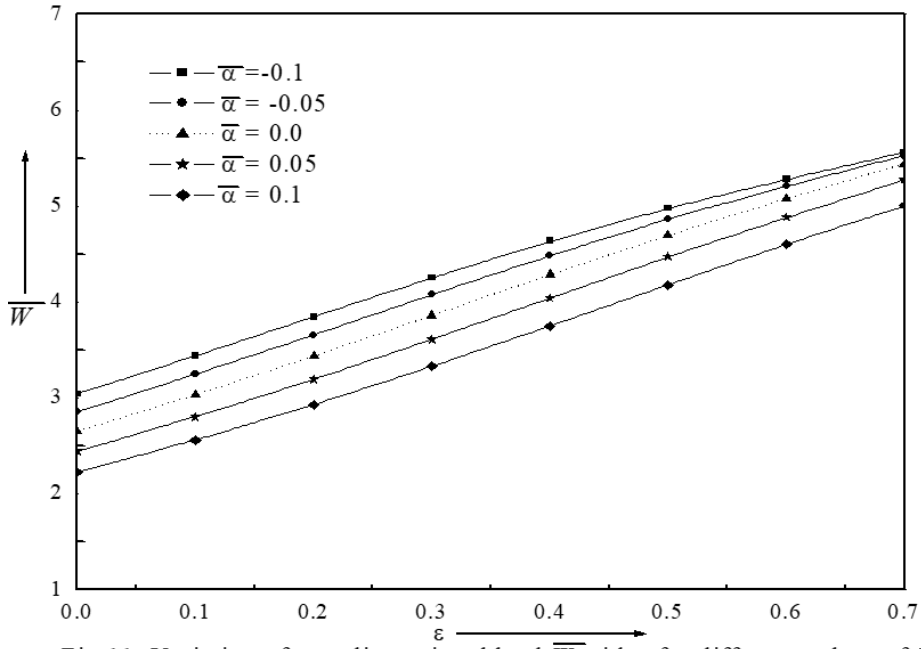

Fig.11. Variation of non-dimensional load $\overline{W}$ with ε for different values of $\overline{\alpha}$ with N = 0.6, $\overline{l}$ = 0.2, ψ = 0.1, $\overline{\varepsilon_1}$ = 0.1, $\overline{\sigma}$ = 0.15 and λ = 0.75.

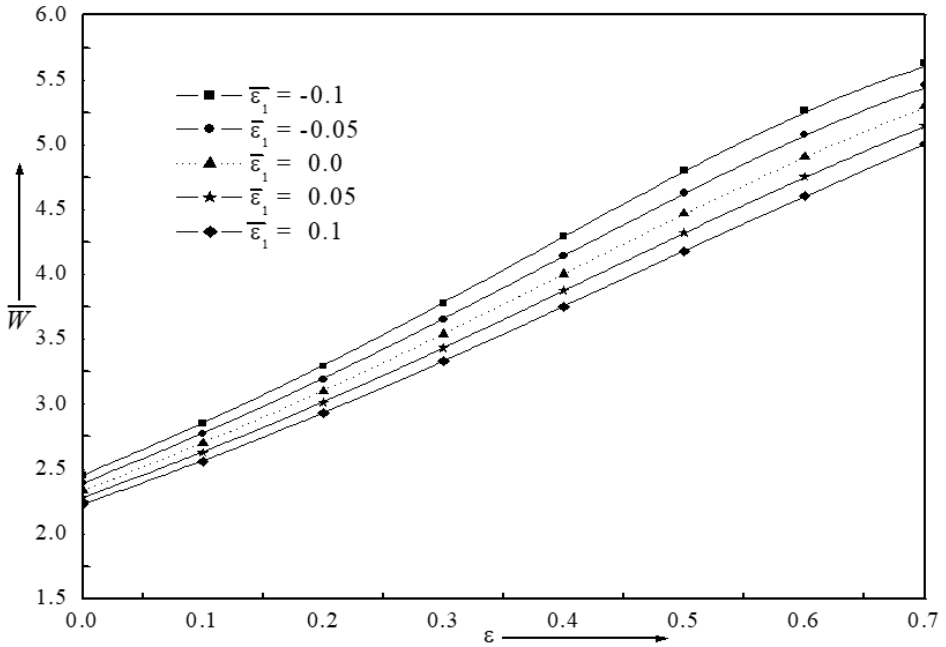

Fig.12. Variation of non-dimensional load $\overline{W}$ with ε for different values of $\overline{\varepsilon_1}$ with N = 0.6, $\overline{l}$ = 0.2, ψ = 0.1 $\overline{\alpha}$ = 0.1, $\overline{\sigma}$ = 0.15 and λ = 0.75.

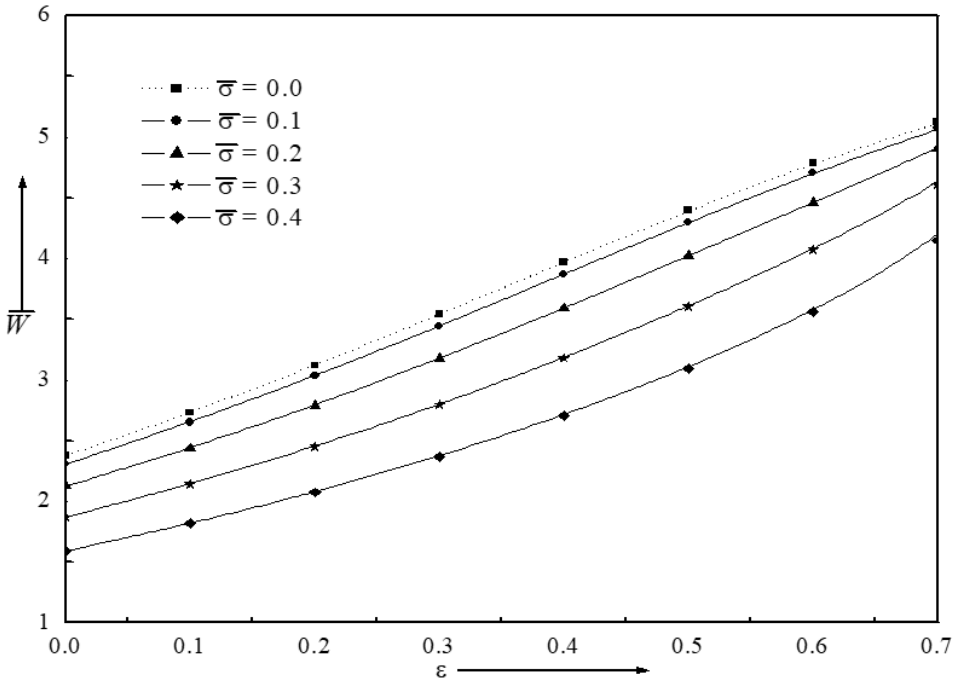

Fig.13. Variation of non-dimensional load $\overline{W}$ with ε for different values of $\overline{\sigma}$ with N = 0.6, $\overline{l}$ = 0.2, ψ = 0.1, $\overline{\alpha}$ = 0.1, $\overline{\varepsilon_1}$ = 0.1 and λ = 0.75.

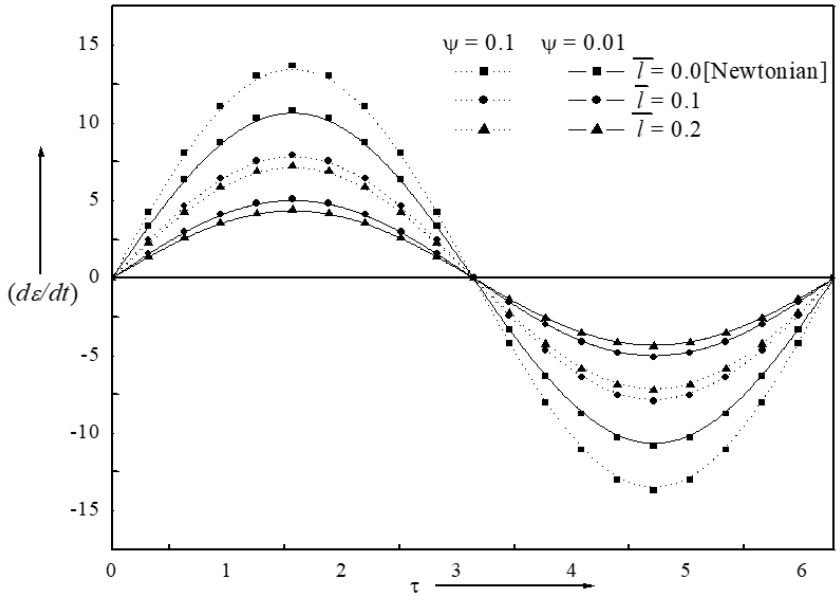

Fig.14. Velocity of the Journal center, ($d\varepsilon/dt$) verses τ for different values of $\overline{l}$ with N = 0.6, $\overline{\alpha}$ = 0.1, $\overline{\sigma}$ = 0.15, $\overline{\varepsilon_1}$ = 0.1, λ = 0.75 ε = 0.2 and s = 0.9.

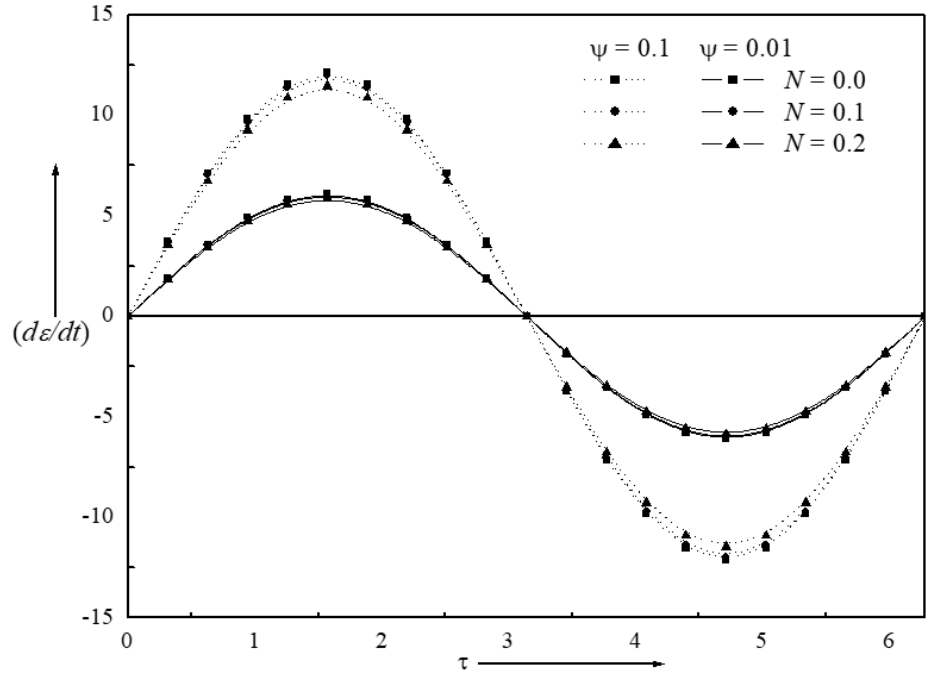

Fig.15. Velocity of the Journal center, ($d\varepsilon/dt$) verses τ for different values of N with $\overline{l}$=0.2, $\overline{\alpha}$= 0.1, $\overline{\sigma}$= 0.15, $\overline{\varepsilon_1}$= 0.1, λ = 0.75, ε = 0.2 and s = 0.9

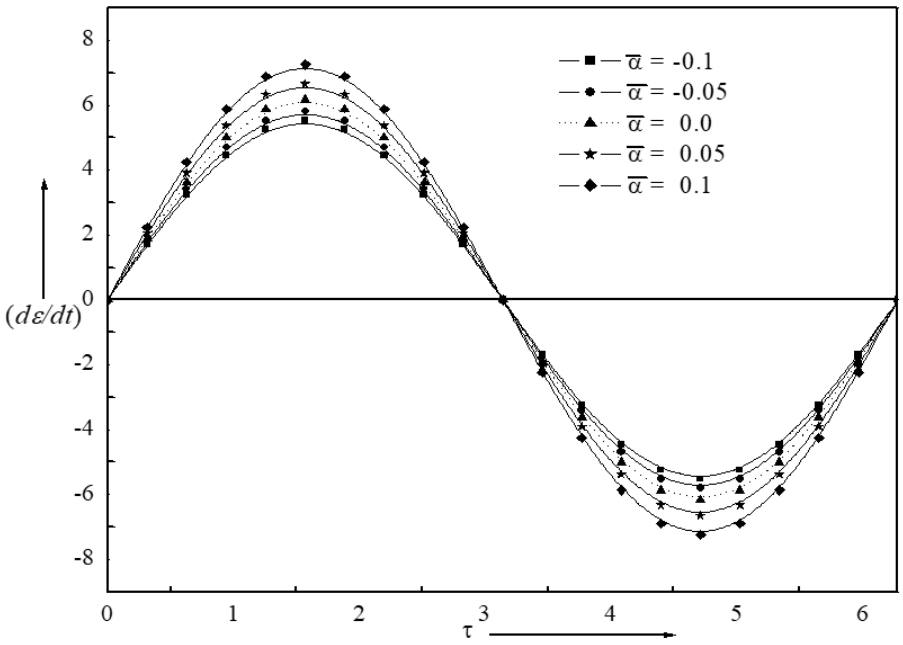

Fig.16. Vecolicty of the Journal center, ($d\varepsilon/dt$) verses τ for different values of $\overline{\alpha}$ with N = 0.6, $\overline{l}$= 0.2, ψ = 0.1, $\overline{\sigma}$= 0.15, $\overline{\varepsilon_1}$= 0.1, λ = 0.75, ε = 0.2 and s = 0.9

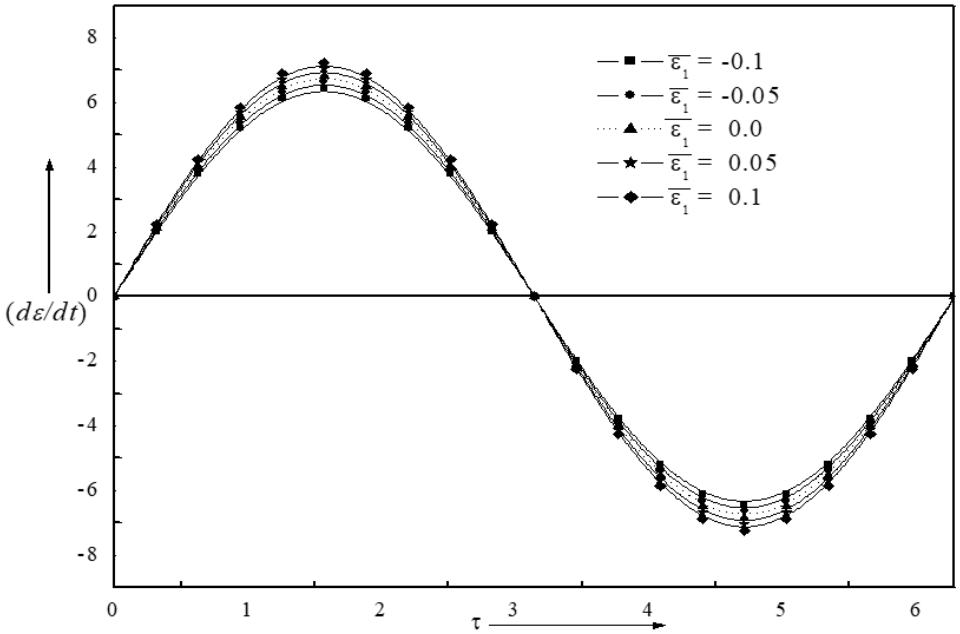

Fig.17. Velocity of the Journal center, $(d\varepsilon/dt)$ verses τ for different values of $\overline{\varepsilon_1}$ with $N = 0.6$, $\overline{l} = 0.2$, $\psi = 0.1$, $\overline{\alpha} = 0.1$, $\overline{\sigma} = 0.15$, $\lambda = 0.75$, $\varepsilon = 0.2$ and $s = 0.9$

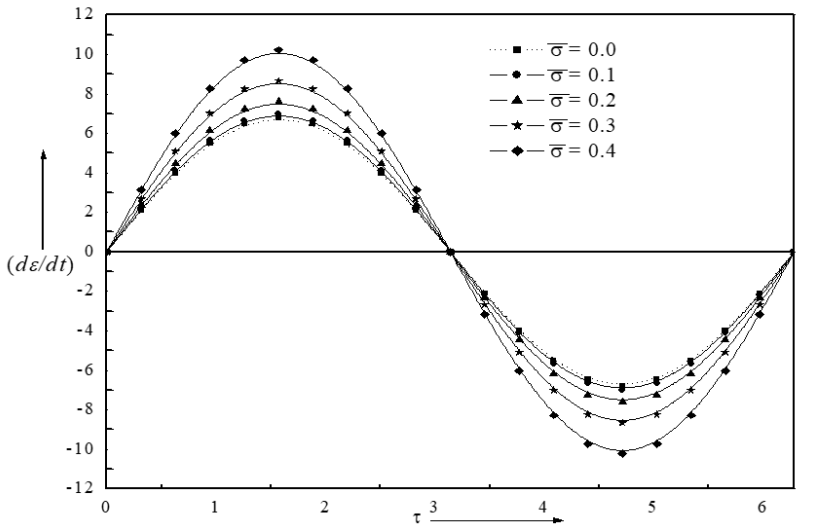

Fig.18. Velocity of the Journal center, $(d\varepsilon/dt)$ verses τ for different values of $\overline{\sigma}$ with $N = 0.6$, $\overline{l} = 0.2$, $\psi = 0.1$, $\overline{\alpha} = 0.1$, $\overline{\varepsilon_1} = 0.1$, $\lambda = 0.75$, $\varepsilon = 0.2$ and $s = 0.9$

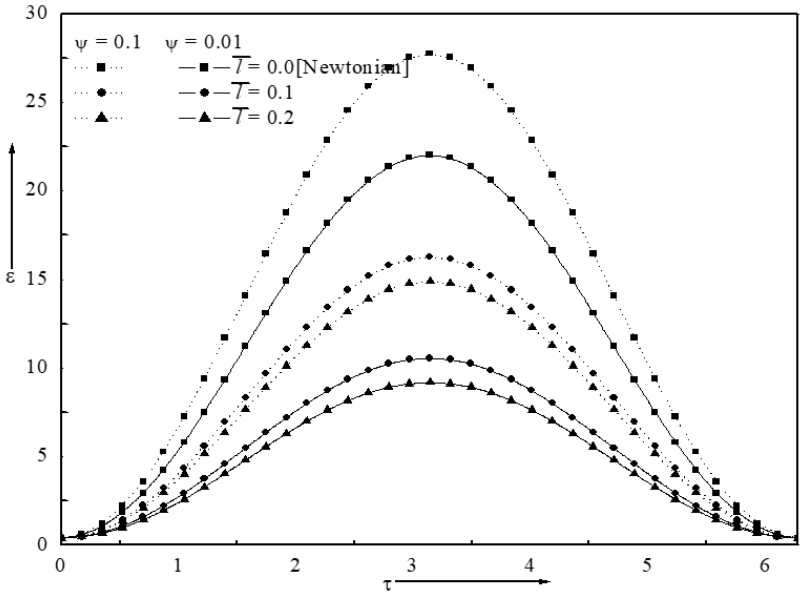

Fig.19. Variation of locus of the journal center ε verses τ for different values of $\overline{l}$ with N = 0.6, $\overline{\alpha}$ = 0.1, $\overline{\sigma}$ = 0.15, $\overline{\varepsilon_1}$ = 0.1, λ = 0.75, ε = 0.2 and s = 0.9

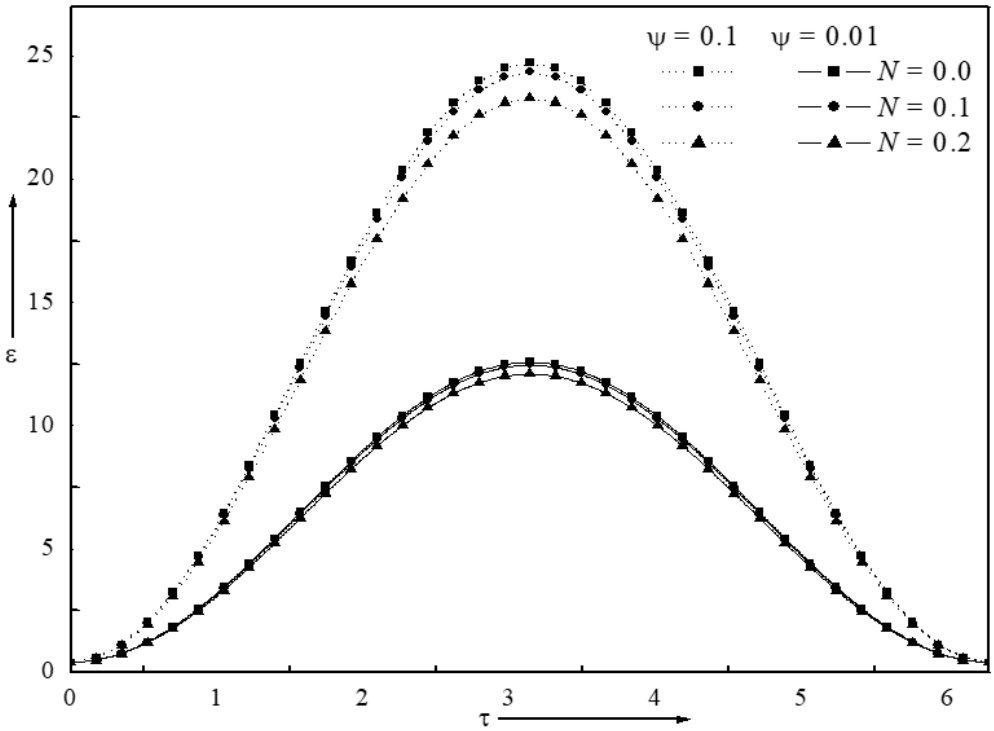

Fig.20. Variation of locus of the journal center ε verses τ for different values of N with $\overline{l}$ = 0.2, $\overline{\alpha}$ = 0.1, $\overline{\sigma}$ = 0.15, $\overline{\varepsilon_1}$ = 0.1, λ = 0.75, ε = 0.2 and s = 0.9

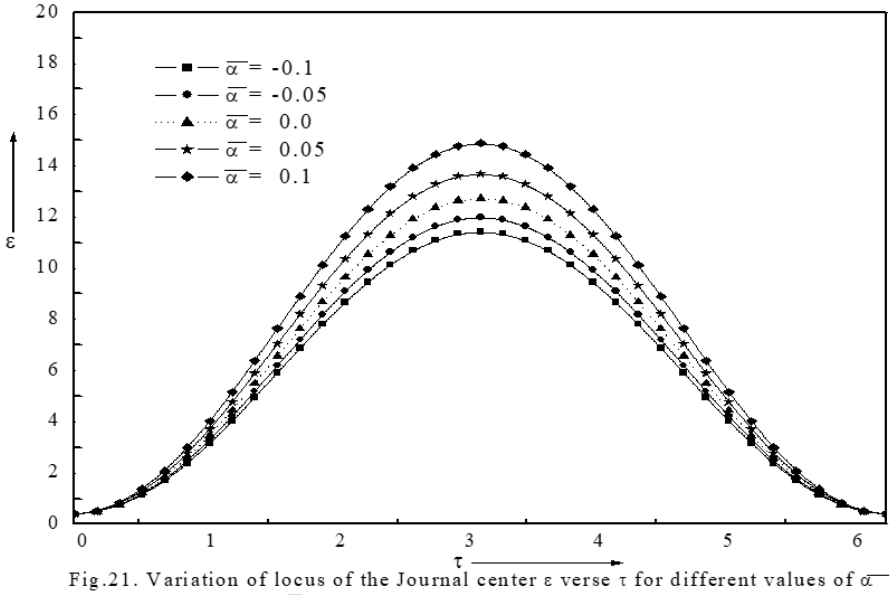

Fig.21. Variation of locus of the Journal center ε verse τ for different values of $\overline{\alpha}$ with $N = 0.6, \overline{T} = 0.2, \psi = 0.1, \overline{\sigma} = 0.15, \overline{\varepsilon_1} = 0.1, \lambda = 0.75, \varepsilon = 0.2$ and s = 0.9

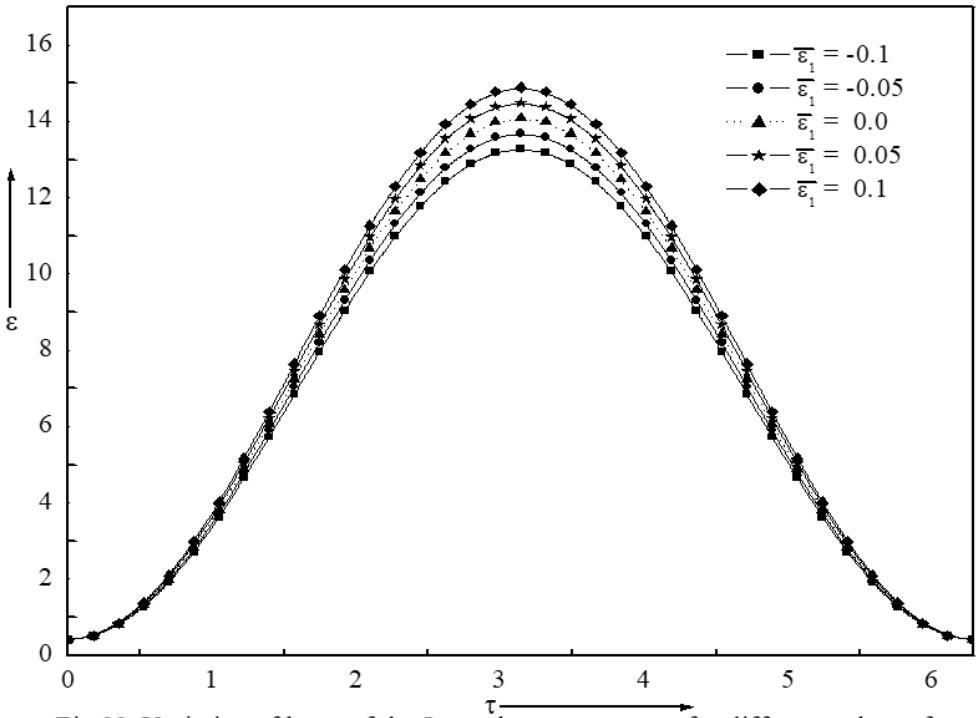

Fig.22. Variation of locus of the Journal center ε verse τ for different values of $\overline{\varepsilon_1}$ with $N = 0.6, \overline{T} = 0.2, \psi = 0.1, \overline{\alpha} = 0.1, \overline{\sigma} = 0.15, \lambda = 0.75, \varepsilon = 0.2$ and s =0.9

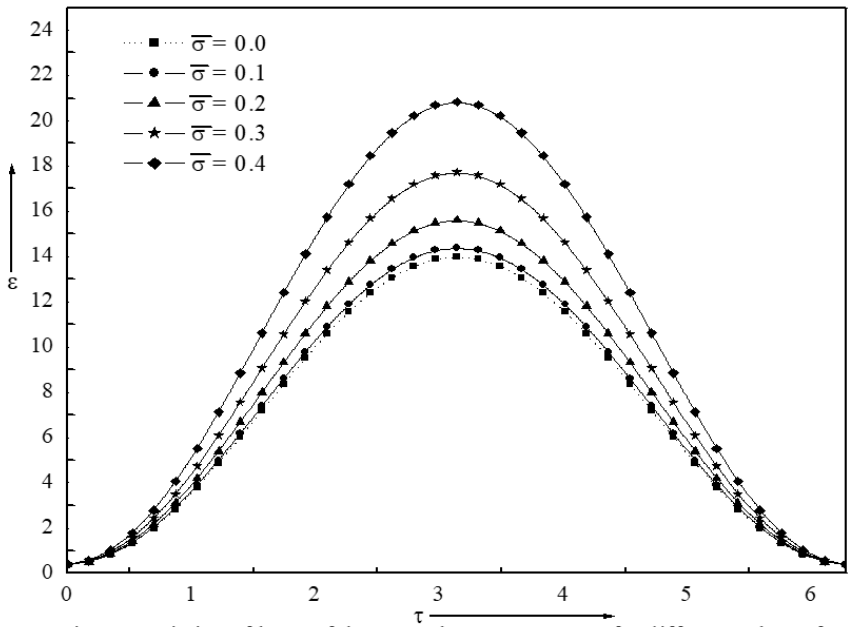

Fig.23. Variation of locus of the Journal center ε verses τ for different values of $\overline{\sigma}$ with $N = 0.6$, $\overline{T} = 0.2$, $\psi = 0.1$, $\overline{\alpha} = 0.1$, $\overline{\varepsilon_1} = 0.1$, $\lambda = 0.75$, $\varepsilon = 0.2$ and s =0.9